Composition-dependent fracture energy in metallic glasses

Hong Li,[1] Jia-Cheng Zhang,[1] Paulo S. Branicio,[2,*] and Zhen-Dong Sha[1,†]
[1]*State Key Laboratory for Strength and Vibration of Mechanical Structures, School of Aerospace Engineering, Xi'an Jiaotong University, Xi'an 710049, China*
[2]*Mork Family Department of Chemical Engineering and Materials Science, University of Southern California, 3651 Watt Way, Los Angeles, California 90089, USA*

(Received 23 October 2022; revised 20 December 2022; accepted 22 February 2023; published 3 March 2023)

The interplay between metallic glasses (MGs) mechanical properties, fracture energy (G), and glass-forming ability (GFA) and their dependence on alloy composition remain poorly understood. Here, we perform molecular dynamics simulations to investigate the intrinsic composition dependence of G in Cu_xZr_{100-x}MGs (x = 20, 30, 40, 50, 64). The results indicate that the value of G increases with Cu content. In addition, it is revealed that MGs with higher G values display higher Poisson's ratio (ν) and GFA, suggesting a close correlation between fracture toughness, mechanical properties, and GFA. This correlation between G, ν, and GFA can be understood based on the fragility (m) of supercooled liquids, which is directly related to the structural heterogeneity in MGs. Larger m values are related to dynamic slowdown and supercooled liquid stabilization, which enhance GFA and the formation of pronounced structural heterogeneity, comprised of loosely packed regions that favor β relaxation and the activation of shear transformation zones. Those concurrently promote the expansion of the plastic zone at the crack tip, enhancing the observed value of G. These simulation results shed light on the intrinsic relationship between fracture toughness, mechanical properties, and alloy composition in MGs.

DOI: 10.1103/PhysRevMaterials.7.035602

I. INTRODUCTION

Composition design is an effective way to improve the mechanical and physical properties of materials. A wide variety of metallic glasses (MGs), ranging from brittle MGs, e.g., Fe-based MGs, to ductile MGs, e.g., Zr-based MGs, have been discovered, indicating that the mechanical properties of MGs are very sensitive to chemical composition. Due to the limited millimeter-scale sample size and room temperature plasticity, a great deal of research is focused on enhancing the glass-forming ability (GFA) and enhancing the plasticity of MGs by tuning the composition and appropriately introducing additional alloying elements [1–4]. The development of bulk MGs and the constant increase in sample dimensions has widened the range of possible structural applications that seek to take advantage of their properties, such as the often displayed outstanding high yield strength and elastic strain [5,6]. In most structural applications, fracture toughness is the primary criterion for selecting materials, above their strength [7]. Therefore, for the commercial application of MGs as structural materials, it is of great interest to investigate the effect of chemical composition on their fracture toughness.

Fracture toughness quantifies a material's ability to resist the propagation of cracks that are inevitably generated during the processing, fabrication, and service of materials. Compared to crystalline materials, the accurate measurement of the toughness of MGs remains a challenge. Even for a given MG composition, reported toughness values vary drastically. For example, literature reports of toughness for $Zr_{41.2}Ti_{12.5}Cu_{10}Ni_{10}Be_{22.5}$ MG samples vary from 16 MPa$\sqrt{\text{m}}$ to over 130 MPa$\sqrt{\text{m}}$ [8]. Such large scatter can be rooted in different causes [9–11]. First, it is challenging to prepare suitable fatigue precracked MG specimens, which is a critical requirement for accurate measurement of fracture toughness. Second, it is also very challenging to have reproducible control of the glassy states in mechanical test samples. Third, accurate and reproducible fabrication of test samples and measurement of their fracture toughness is also challenging due to strict protocols, specific sample dimensions, and combined effects of intrinsic and extrinsic factors [11]. All of these factors prevent reliable and reproducible fracture toughness measurements. Therefore, seeking effective methods for predicting fracture toughness has been a topic of high interest.

Akin to crystalline materials, attempts have been made to correlate fracture toughness with the mechanical properties of MGs, such as the Poisson's ratio (ν), which reflects the competition between the resistance to changes in interatomic bond angle (shear) and bond length (dilatation). A high ν value generally indicates low resistance to plastic deformation and high resistance to crack opening. Many studies have revealed that fracture toughness correlates with ν for a range of MG alloys, with a sharp brittle-to-ductile transition occurring at a critical value $\nu \sim 0.315$ [12–14]. Although this empirical rule has been successfully applied to design MGs with high plasticity, some reported results deviate from its prediction. For example, some Au- and Pd-based MGs exhibit a brittle behavior, despite displaying ν values exceeding 0.39 [15]. Furthermore, Madge *et al.* have reported that mode II toughness increases

*Corresponding author: branicio@usc.edu
†zhendongsha@mail.xjtu.edu.cn

with ν, rather than displaying an abrupt transition at a critical ν value [16]. These results suggest that the proposed universal correlation between ν and fracture toughness remains controversial. In addition, studies have shown that fracture toughness is associated with GFA. For instance, Ketkaew *et al.* reported that the observed mechanical toughening transition is similar to MG glass transition [10]. Shao *et al.* have examined a broad range of 13 MGs of different alloy systems to explore the effect of chemical composition on the fracture toughness of MGs and found that fracture toughness is associated with both ν and GFA [17]. Although the correlation between the fracture toughness and characteristic parameters measured for the MGs, such as ν and GFA, was established, the underlying sources for the relation among them remain elusive.

Many studies have been carried out for the binary Cu-Zr MG system due to its wide glass-forming composition range and desirable mechanical properties. However, to the best knowledge of the authors, a systematic study of the fracture toughness of the binary Cu-Zr MG system is still missing, preventing the investigation of the correlation between fracture toughness and other properties. In this work, we perform molecular dynamics (MD) simulations to understand how fracture energy (G) changes with composition in Cu_xZr_{100-x}MGs ($x = 20$, 30, 40, 50, 64). We then focus on the correlation between G, ν and GFA. Furthermore, the common underlying origin of the relationship is explored and discussed.

II. METHODS

A. MD simulations

All MD simulations are carried out using the large-scale atomic/molecular massively parallel simulator (LAMMPS) [18,19]. A Nose-Hoover thermostat and a Parrinello-Rahman barostat control the system temperature and pressure, respectively [20,21]. The embedded atom method (EAM) potential for Cu-Zr alloys developed by Cheng *et al.* is used to describe the atomic interactions [22]. A constant integration time step of 2 fs is applied in all simulations. The CuZr samples are generated as detailed in previous reports [23,24]. First, to simulate Cu_xZr_{100-x}MGs ($x = 20$, 30, 40, 50, 64), a small MG structure consisting of a $6.2 \times 6.2 \times 6.2\,\text{nm}^3$ cube with the same number of Cu and Zr atoms arranged in the $B2$ structure is created. Then an appropriate amount of Cu or Zr atoms is randomly substituted by atoms of the opposite type base on the desired composition. After that, the small MG sample is equilibrated at 2000 K for 2 ns in the isothermal-isobaric ensemble (*NPT*) and then cooled down to 300 K using a cooling rate of 10^{10} K/s. Finally, a large MG sample with dimensions of $100.0(W) \times 31.2(L) \times 6.2\,(B)\text{nm}^3$ is constructed by replicating the small MG sample, which is then annealed in the *NPT* ensemble at a temperature slightly above the glass transition temperature (T_g) to eliminate artificial patterns introduced during the replication process before it is finally cooled to 50 K. In all *NPT* simulations, the external pressure is set at zero. In addition, our previous work has also demonstrated that when W is above 50 nm, the measured G value is independent of W [11].

In order to measure the value of G, a semicircular notch with a radius of 1.25 nm is introduced on one edge of the sample at the middle of the sample length, as shown in Fig. 1(a). The notch depth is half the sample width, i.e., 50 nm. In our previous work, it has been demonstrated that the measured G is independent of the notch shapes in the range of sizes considered [11]. Before loading, the notched MG sample is further relaxed for 50 ps. During uniaxial tensile loading, the periodic boundary conditions are applied in the z direction, while free boundary conditions are used in the other two directions. A constant strain rate of $4.0 \times 10^8\,\text{s}^{-1}$ is imposed on the top and bottom layers ($\sim$0.54 nm) in the y direction, which are set as semirigid holders to avoid undesired stress concentration [14]. The *NVE* ensemble is used in the semirigid layers, and the *NPT* ensemble is used in other regions of the sample.

B. Measurement of G

The G measurement approach is illustrated in Fig. 1, which follows the approach proposed by Deng *et al.* for measuring G values for MGs ranging from brittle to ductile [14]. In this method, two samples (one notched and one unnotched) are simultaneously prepared. The notched MG sample is used to determine the critical elongation (u_c) when crack extension occurs. By monitoring the evolution of the atomic number density, ρ_N, in a semicircular region with a radius of 4.05 nm ahead of the notch tip during tensile deformation, u_c can be identified when the value of ρ_N drops sharply, as shown in Fig. 1(b). The unnotched MG sample is used to determine the work done $\prod(u_c)$, calculated by the area beneath the force-elongation curve (P-u) of the unnotched sample up to u_c, as shown in Fig. 1(c). The value of G is calculated as

$$G = \frac{\prod(u_c)}{BW}, \tag{1}$$

where B and W are the thickness and width of the sample, respectively.

III. RESULTS AND DISCUSSION

A. G in Cu-Zr MGs

To validate the structural characteristics of amorphous metals, we utilized the pair distribution function (PDF) and static structure factor $S(q)$ as our primary analysis tools. Figure 2(a) shows the PDFs of Cu_xZr_{100-x}MGs ($x = 20$, 30, 40, 50, 64) at 300 K. A split of the second peak in the PDF curves indicates that the rapidly solidified Cu_xZr_{100-x} alloy solids display amorphous characteristics (marked with red arrow), which are due to the enhancement of the atomic ordering during the transition from liquid to amorphous state [25,26]. In addition, with the increase of Cu content, both the position of the peaks and the shape of the PDFs are changed, which is in agreement with experimental results [27]. The first peak of the PDFs splits into two inflection points (marked with a black arrow). Mattern *et al.* have pointed out that the shape of the first maximum exhibits very strong composition dependence, which is caused by the different contributions of Cu-Cu, Cu-Zr, and Zr-Zr pairs to the total PDF functions [28]. Figure 2(b) shows the $S(q)$ curves of Cu_xZr_{100-x}MGs ($x = 20$, 30, 40,

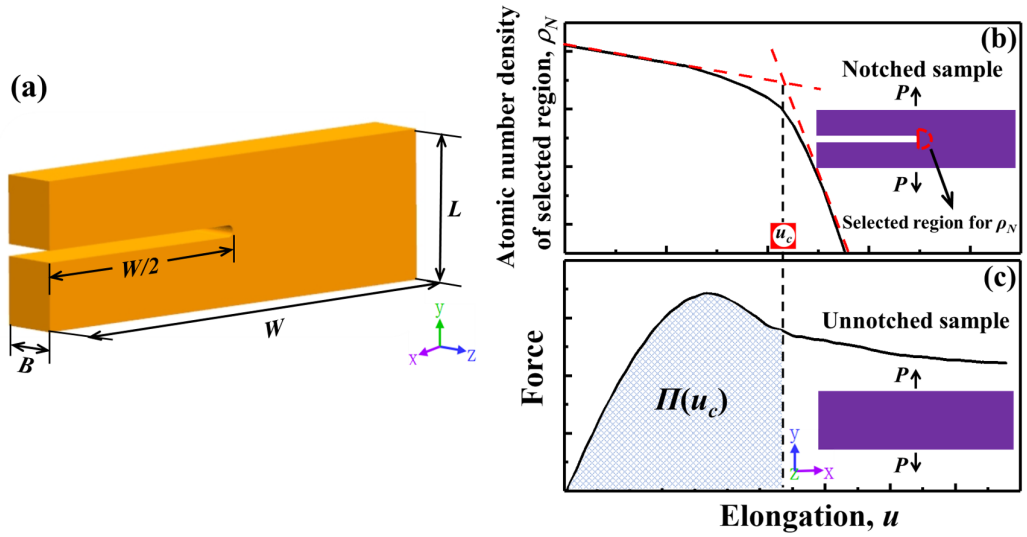

FIG. 1. (a) Illustration of the single-edge notched MG simulation model. The slab model features a pre-existing notch with a depth set at half the sample width. (b),(c) Schematic diagram of the G measurement approach. (b) The notched sample is employed to determine u_c, which is identified from the intersection of the two linear fitting lines. When the value of ρ_N ahead of the notch tip drops steeply, the crack extension occurs. (c) The P-u curve of the unnotched sample is used to determine the work done $\prod(u_c)$ up to u_c.

50, 64) calculated by the Debye's equation. The studied MGs display a similar $S(q)$ to that of typical amorphous alloys, with diffuse peaks and a decreasing intensity as q increases. The curved shapes observed are consistent with those previously reported in the literature [29]. The calculated PDFs and $S(q)$ indicate that the EAM potential utilized in our study is well suited to describe the interatomic interactions in the Cu-Zr binary alloys. Notably, the first peak position of $S(q)$ shifts towards higher q as Cu content increases [see Fig. 2(b)]. These shifts in peak position correspond to a volume shrinkage and density increase caused by the increase in Cu content. This change in volume and density is proposed to relate to specific types of short-range order [30,31].

Recent reports indicate that the fracture toughness of MGs has a strong dependence on composition within a given alloy family [17]. Here, we examine how G changes with composition in Cu_xZr_{100-x} MGs, using identical sample and notch configurations. The primary reason for using the binary Cu-Zr MGs is the reported high GFA for unusually wide glass-forming composition ranges [29,32]. Thus, samples of sufficiently large dimensions can be obtained to meet the requirements of standard samples used for measuring fracture toughness [33]. For the samples considered, the measured G value increases with increasing Cu content, as shown in Fig. 3. The maximum value, $G = 5.13\,\mathrm{J/m^2}$, corresponding to 64.5 at.% Cu is 53% higher than the value predicted for ductile MGs, $3.35\,\mathrm{J/m^2}$, in MD simulations of model MGs using the same methodology employed here [14]. Previous investigations have demonstrated that $Cu_{64}Zr_{36}$ is the best glass-forming composition within Cu-Zr alloys [34]. Therefore, the results obtained here imply that $Cu_{64}Zr_{36}$ exhibits the best combination of GFA and fracture toughness, which suggests that it is possible to concurrently optimize the GFA and the toughness of MGs.

The measured G value in experiments exhibits extensive fluctuation due to the combined effects of intrinsic and extrinsic factors such as sample processing conditions, geometries, and testing conditions. In contrast, MD simulations allow for

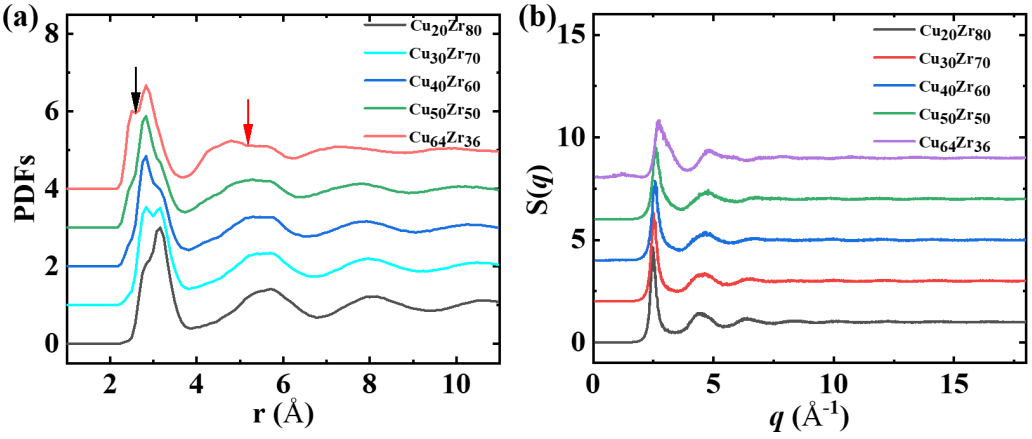

FIG. 2. (a) The pair distribution function (PDF) of the Cu_xZr_{100-x}MGs. (b) The static structure factor $S(q)$ of Cu_xZr_{100-x}MGs.

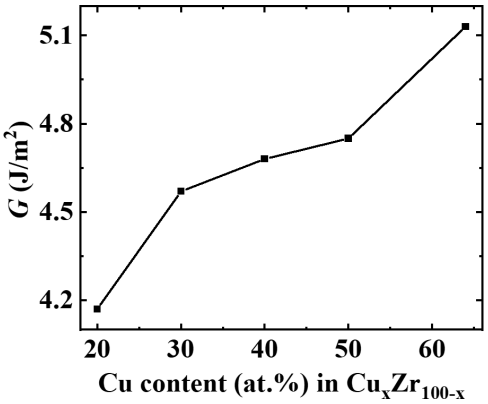

FIG. 3. Dependence of fracture energy G on Cu concentration in Cu-Zr MGs.

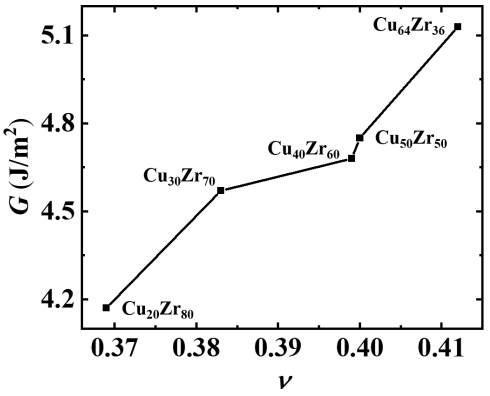

FIG. 4. Correlation between G and ν in Cu-Zr MGs.

independent and accurate control of these variables, resulting in a lower error compared to experimental tests. Therefore, we expect the error of G, measured in MD, to be negligible under the same conditions. To demonstrate that the error is negligible, we conducted two additional simulations using statistically distinct models generated from different initial configurations to calculate G for a $Cu_{50}Zr_{50}$ MG. The calculated G values are 4.745, 4.751, and 4.779 J/m^2, respectively. Here, our focus is on the calculated error, which we evaluated in terms of the standard deviation. The calculated standard deviation of G is less than 1.8%, indicating that the error of measured G in MD can be neglected.

B. Correlation among G, GFA, and ν

The value of ν is expected to be a useful quantity in the search for tough MGs, since it is widely accepted that a critical ν value is associated with reported brittle-to-ductile (BTD) transitions in MGs [9,12–14,16,35]. Here, we aim to verify if the proposed correlation between toughness and ν is valid for Cu-Zr MGs. The ν is obtained by the following expression:

$$\nu = \frac{1}{2} - \frac{3}{6B/G + 2}, \tag{2}$$

where $B = \frac{1}{3}(C_{11} + 2C_{12})$ is the bulk modulus, $G = \frac{1}{2}(C_{11} - C_{12})$ is the shear modulus, and C_{ij} is the elastic tensor. Akin to the G, the ν increases with an increasing Cu content in Cu-Zr MGs. Mendelev *et al.* have reported similar trends, observing an increase in ν with Cu concentration in the range $33.3 \leqslant x \geqslant 64.5$ for Cu_xZr_{100-x}, resulting in a small range of values from 0.41 to 0.425. However, the range of ν values in this study (0.369–0.41) is significantly different due to variations in the empirical potential and cooling rate used in the preparation of the MGs samples [36]. Fig. 4 shows that the value of G increases monotonically with ν. From this, it can be seen that higher toughness can be expected with higher values of ν for Cu-Zr MGs, which can be understood in terms of the competition between shear banding and cracking. Higher ν values cause the tip of shear bands to extend rather than develop into a crack, which can effectively increase the size of the plastic zone (R_p) at the crack tip, thus favoring elevated toughness [37]. In MGs, shear transformation zones (STZs) act as the basic carriers of plasticity, which can be monitored directly by measuring the fraction of atoms with relatively large atomic shear strain ($\eta_i^{\text{Mises}} > 0.2$) [38]. At the onset of crack extension, the plasticity carried by STZs is constrained ahead of the notch tip. Therefore, calculating the fraction of atoms with relatively large atomic shear strain can quantitatively evaluate the R_p. The larger the fraction, the higher the R_p, indicating the high density of STZs and the development of plastic deformation. The trend of the effect of Cu content on the R_p measured at u_c is displayed in Fig. 5. It should be noted that a different threshold η_i^{Mises} will not affect the observed tendency. It is seen that R_p shows a similar composition dependence as ν. Moreover, it is noteworthy that the values of ν for all the specimens are above the universal proposed critical ν value of 0.31 to 0.32 for the BTD transition [14]. The results suggest that the critical value of ν seems to be related to alloy chemistry.

Previous studies have shown that the toughness of MGs is closely correlated with their GFA, and whether the correlation is positive or negative depends on the specific bonding characteristics [17]. In order to investigate this correlation in Cu_xZr_{100-x}MGs, we consider the variation in GFA over a broad composition range within $20 \leqslant x \geqslant 64$. The GFA is evaluated by the reduced glass transition temperature ($T_{rg} = T_g/T_L$) [39,40], which was proposed by Turnbull *et al.* based on the classical nucleation theory [41]. The T_L is the melting temperature of crystal alloys. A larger T_{rg} corresponds to a better GFA. The values of T_g and T_L are determined

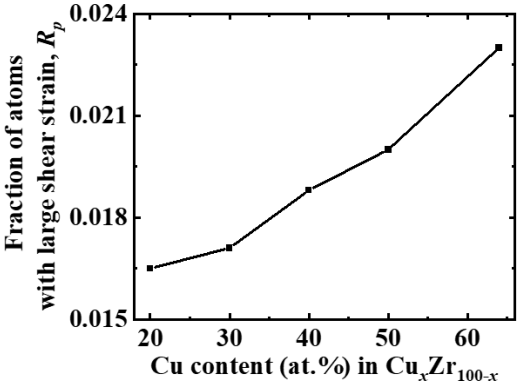

FIG. 5. Fraction of atoms with relatively large atomic shear strain at u_c, corresponding to the R_p, as a function of Cu content.

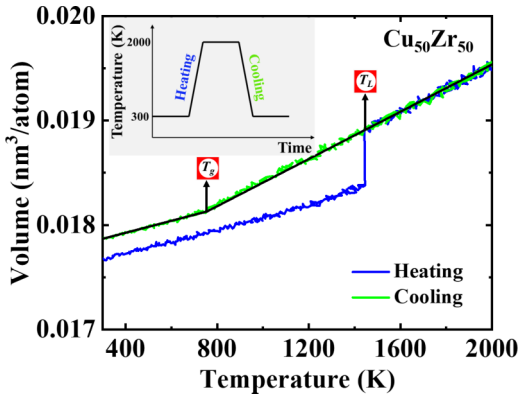

FIG. 6. Volume change as a function of temperature during heating and cooling of $Cu_{50}Zr_{50}$. The glass transition temperature T_g and melting point T_L are indicated. The inset shows the thermal loading schedule. T_g corresponds to the inflection point during cooling, while T_L corresponds to the volume discontinuity observed during heating.

in the simulations from the dependence of the volume on temperature during heating and cooling, as shown for the $Cu_{50}Zr_{50}$ sample in Fig. 6. The inset in Fig. 6 exhibits the thermal loading schedule used. The Cu-Zr alloy is heated from 300 to 2000 K and then held for 0.2 ns for better homogeneity and stability. Subsequently, the system is quenched to 300 K. The heating and cooling processes are conducted at the same rate of 10^{10} K/s at zero external pressure. The *NPT* ensemble is used in the simulation process. Figure 6 shows that the glassy state with more free volume after cooling has a higher volume than the initial crystalline state. The T_L value is estimated by the temperature corresponding to the discontinuous change in volume during heating. The T_g value is estimated by monitoring the inflection point in the volume versus temperature curve during the quenching process. For any given composition, three simulations with different initial configurations are performed to estimate T_{rg} to ensure reliable statistical results. The results shown in Fig. 7 indicate that T_{rg} increases with Cu content. The calculated T_{rg} values exhibit a significant variation of over 16% with changes in composition, which is higher than the calculated error of approximately 5%. Moreover, the calculated T_{rg} values of the

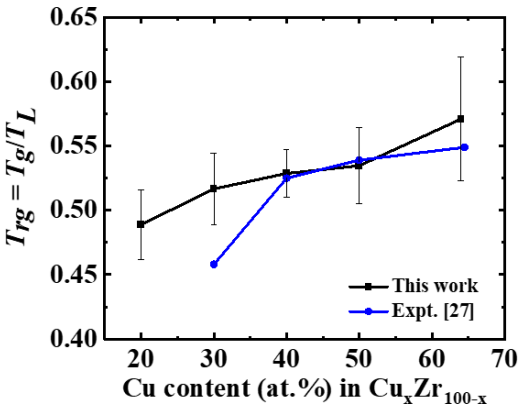

FIG. 7. Dependence of the reduced glass transition temperature T_{rg} on Cu concentration in Cu-Zr MGs.

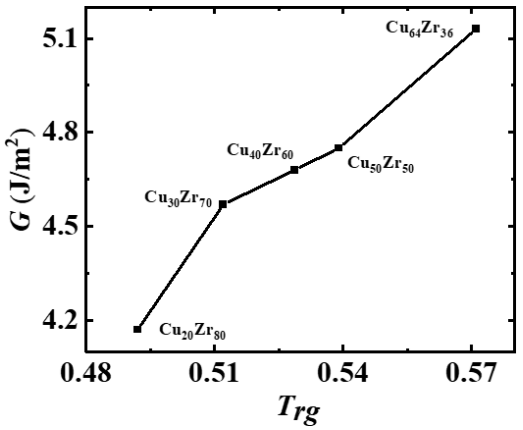

FIG. 8. Dependence of G on the reduced glass transition temperature T_{rg} in Cu-Zr MGs.

components and their dependence on composition are in good agreement with the available experimental data [27,29] and previous MD simulations results [42]. A correlation of G with T_{rg} for the Cu-Zr MGs is shown in Fig. 8. The value of G has a similar correlation with T_{rg} as that found with ν, i.e., implying that the value of G increases with GFA. As mentioned above, the $Cu_{64}Zr_{36}$ MG exhibits the best combination of GFA and toughness. The results indicate a close relationship between toughness and GFA for the Cu-Zr MGs.

C. Underlying origin of the correlation among G, GFA, and ν

It is noteworthy that the calculated trend of G with composition follows a similar trend as ν and GFA, indicating that they have a common origin. Such origin may be buried deep in the structure and properties of the supercooled liquid state since the structure and properties of the glass state derive directly from it. Numerous studies have shown that ν and GFA correlate well with kinetic fragility (m) [43–45]. In order to further investigate the physical origin of the correlation among G, ν, and GFA, we calculate the value of m as a function of composition in the Cu-Zr MGs. The m first proposed by Angell *et al.* divides glass-forming liquids into strong and fragile based on the degree of departure from the Arrhenius behavior at T_g, which is closely related to the slowing down of the dynamics, such as relaxation time and viscosity [46]. A large m value is associated with "fragile" liquids, exhibiting a significant deviation from the Arrhenius behavior, while "strong" liquids follow an Arrhenius-like behavior. Quantitatively, m is most commonly defined in terms of shear viscosity (η) or structural relaxation time (τ_a),

$$m = \left.\frac{d\log_{10}(\tau_a)}{d(T_g/T)}\right|_{T=T_g} = \left.\frac{d\log_{10}\eta}{d(T_g/T)}\right|_{T=T_g}. \quad (3)$$

Here, the value of m is quantified in terms of τ_a, while the value of τ_a can be estimated by the self-intermediate scattering function (SISF) [47], defined as follows:

$$F_s(q,t) = \frac{1}{N}\sum_{i=1}^{N}\langle \exp\left(iq[r_i(t) - r_i(0)]\right)\rangle, \quad (4)$$

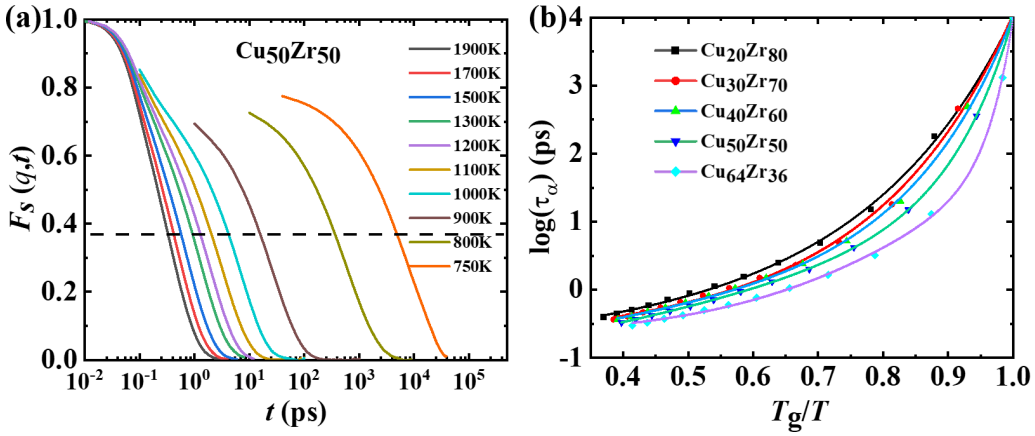

FIG. 9. (a) Self-intermediate scattering function of $Cu_{50}Zr_{50}$ glass-forming liquids at different temperatures. The τ_a is determined as the $F_s(q,t)$ decays to e^{-1} labeled by the horizontal dashed line. (b) τ_a as a function of inverse temperature scaled by T_g for Cu-Zr MGs.

where N is the number of atoms. The q is the wave vector and is usually fixed at $q_{\max} = |\vec{q}|$, corresponding to the first peak position of the structure factor [48]. The r_i represents the location of the atom i. Taking the $Cu_{50}Zr_{50}$ MG as an example, the evolution of $F_s(q,t)$ with time for glass-forming liquids at different temperatures is shown in Fig. 9(a). The τ_a corresponds to the time when the SISF decays to e^{-1} marked with the horizontal dashed line in Fig. 9(a) [49]. In addition, previous studies have suggested that T_g is set as the temperature when τ_a reaches 10^4 ps, which is consistent with that obtained from the volume-temperature curve [50]. For example, Fig. 9(a) shows that the temperature corresponding to $\tau_a = 10^4$ ps is about 750 K, which agrees well with 755 K of T_g obtained from the volume-temperature curve for $Cu_{50}Zr_{50}$ MG. Figure 9(b) shows the $\log(\tau_a)$ as a function of inverse temperature scaled by T_g for the Cu-Zr MGs. The values of m are calculated using Eq. (3), as shown in Table I. The value of m also increases with Cu content, which is consistent with previous reports for Cu-Zr MGs [51].

From the above observations, we can conclude that larger m values correspond to larger values of both ν and GFA for the studied Cu-Zr MGs. Such a positive correlation between m and ν agrees with previous results [43], which reported that MGs with higher ν tend to be more fragile. It should be noted that fragile glasses generally exhibit larger dynamic heterogeneity, which indicates the existence of large transient spatial fluctuations in the local dynamical behavior [52–54]. Some studies have revealed that larger dynamic heterogeneity is closely linked to higher structural heterogeneity, consisting of loosely packed regions, which promote β relaxations and STZs, leading to the formation of shear bands [35,53,55]. The observed high toughness of MGs is closely related to the formation and generation of a high density of shear bands at the crack tip, extending the plastic zone [56,57]. Therefore, the fragile supercooled liquid state, associated with higher structural heterogeneity, can serve as a link to understanding the correlation between G and ν.

It is worth noting that a correlation between fragility and GFA has been found in many MGs. Our results show that high fragility correlates with a high GFA in the Cu-Zr MGs, in agreement with other reports in the literature [54,58]. For example, Tang *et al.* reported that better GFA corresponds to larger m and that the glass formation criteria of multicomponent alloys with composition near deep eutectic do not apply to binary MGs [58]. However, our results contrast with the view that a high GFA is associated with a strong liquid behavior, as reported in other investigations [59]. A strong liquid usually has a higher viscosity across the glass transition region, slowing the crystallization kinetics and leading to high GFA.

Nevertheless, some studies pointed out that viscosity alone cannot provide a satisfactory explanation for the GFA of MGs [60]. Nevertheless, GFA closely correlates with dynamic heterogeneity [54,61,62]. Large dynamic heterogeneity coupled with structural heterogeneity tends to slow the dynamics and stabilize the undercooled liquid, enhancing the GFA. Therefore, the relationship between GFA and m observed in this study can be attributed to dynamic heterogeneity. On the other hand, larger m values are associated with higher structural heterogeneity, which promotes the development of the plastic zone in front of the crack tip, thereby enhancing the value of G [53,56,57]. As a result, the fragile state with higher structural heterogeneity can explain the observed correlation among G, ν, and GFA in this study.

TABLE I. Calculated fragility m for Cu-Zr glass-forming liquids.

Amorphous alloys	$Cu_{20}Zr_{80}$	$Cu_{30}Zr_{70}$	$Cu_{40}Zr_{60}$	$Cu_{50}Zr_{50}$	$Cu_{64}Zr_{36}$
m	19	22	24	33	62

D. Variation in atomic structure

In general, the intrinsic mechanical properties of MGs are controlled by their internal atomic-level structure. To reveal a one-to-one structure-property correlation, we probe the variations in structural features with the composition by analyzing the atomic Voronoi polyhedra. A Voronoi polyhedron is described by a set of indexes $\langle n_3, n_4, n_5, n_6\rangle$, where n_i denotes the number of i-edged faces of the polyhedron. For example, the polyhedra with Voronoi index $\langle 0, 0, 12, 0\rangle$ has 12 pentagons enclosed to form an icosahedral cluster with a

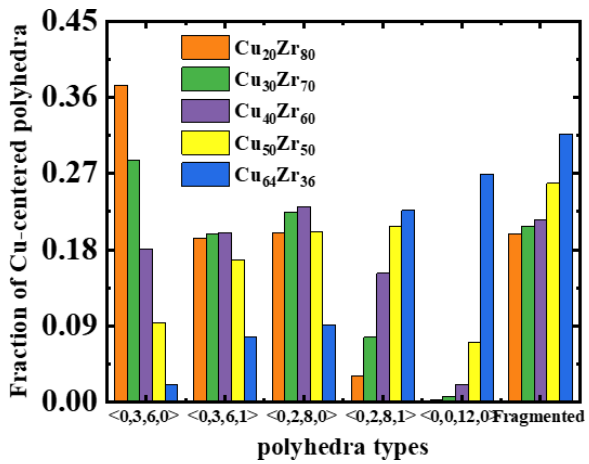

FIG. 10. Fraction of various Cu-centered Voronoi polyhedral for the Cu-Zr MGs.

high degree of fivefold symmetry, which is defined as a "full icosahedron" (FI). The fractions of the five most prevalent Cu-centered Voronoi polyhedra in Cu_xZr_{100-x} MGs are shown in Fig. 10. The remaining Voronoi polyhedra types are grouped together and referred to as "fragmented polyhedra" hereafter. We focused on the FI and fragmented polyhedra changes, which are the key local structural motifs in MGs. It has been reported that FI clusters are the most stable geometrical units and the most resistant to shear transformations (STs) [63]. In contrast, the fragmented polyhedra usually have a "liquidlike" nature and are more prone to participate in STs [64]. Our results show that both FI and fragmented polyhedra increase monotonically with Cu content, as shown in Fig. 10. It is well known that a larger FI fraction in an MG contributes to its structural stability as well as its strength. On the other hand, an increase in the fragmented polyhedral is expected to promote the generation of STs to accommodate plastic strain. Moreover, it should be noted that the work done $\prod(u_c)$ by the external load is calculated by the area beneath the P-u curve, the measured G depends on both the plastic deformation and strength. Therefore, the increase of FI and fragmented polyhedral can explain the above-observed enhanced G value with increasing Cu content.

IV. CONCLUSIONS

In summary, the dependence of G on Cu_xZr_{100-x} MGs ($x = 20$, 30, 40, 50, 64) is studied using MD simulations. Our results show that the value of G increases with Cu content. Furthermore, the correlation among G, ν, and GFA is established. It is found that larger G values are associated with larger ν and GFA, implying a close relationship between toughness, mechanical properties, and GFA. The correlation among G, ν, and GFA can be understood considering the glass fragility m, which is associated with the structural heterogeneity of MGs. Larger m can slow down the dynamics of supercooled liquids, enhancing GFA, resulting in a high degree of structural heterogeneity, meanwhile promoting activation of STZs and the formation of plastic zone ahead of the crack tip, thereby enhancing the G of MGs. Furthermore, the structural analysis indicates that the enhancement of the G value with increasing Cu content is rooted in the concomitant increase of FI and fragmented polyhedral. While Cu-Zr MGs have been widely used as a representative of ductile MGs, it should be noted that other MGs exhibit distinct characteristics due to variations in chemical bonding strength and coordination/connectivity. Therefore, caution must be exercised in extrapolating the conclusions of our paper to other MGs.

ACKNOWLEDGMENT

The authors would like to acknowledge the financial support by the National Natural Science Foundation of China, through Grants No. 12102325 and No. 11972278.

[1] L. Yang, G. Q. Guo, L. Y. Chen, C. L. Huang, T. Ge, D. Chen, P. K. Liaw, K. Saksl, Y. Ren, Q. S. Zeng, B. LaQua, F. G. Chen, and J. Z. Jiang, Atomic-scale Mechanisms of the Glass-Forming Ability in Metallic Glasses, Phys. Rev. Lett. **109**, 105502 (2012).

[2] Q. Wang, C. T. Liu, Y. Yang, J. B. Liu, Y. D. Dong, and J. Lu, The atomic-scale mechanism for the enhanced glass-forming-ability of a Cu-Zr based bulk metallic glass with minor element additions, Sci. Rep. **4**, 4648 (2014).

[3] Y. Y. Zhao, A. Inoue, C. Chang, J. Liu, B. Shen, X. Wang, and R. W. Li, Composition effect on intrinsic plasticity or brittleness in metallic glasses, Sci. Rep. **4**, 5733 (2014).

[4] L. Zhang, Y. Q. Cheng, A. J. Cao, J. Xu, and E. Ma, Bulk metallic glasses with large plasticity: Composition design from the structural perspective, Acta Mater. **57**, 1154 (2009).

[5] J. J. Kruzic, Bulk metallic glasses as structural materials: A review, Adv. Eng. Mater. **18**, 1308 (2016).

[6] M. F. Ashby and A. L. Greer, Metallic glasses as structural materials, Scr. Mater. **54**, 321 (2006).

[7] M. E. Launey and R. O. Ritchie, On the fracture toughness of advanced materials, Adv. Mater. **21**, 2103 (2009).

[8] W. Chen, H. Zhou, Z. Liu, J. Ketkaew, N. Li, J. Yurko, N. Hutchinson, H. Gao, and J. Schroers, Processing effects on fracture toughness of metallic glasses, Scr. Mater. **130**, 152 (2017).

[9] J. Xu, U. Ramamurty, and E. Ma, The fracture toughness of bulk metallic glasses, JOM **62**, 10 (2010).

[10] J. Ketkaew, W. Chen, H. Wang, A. Datye, M. Fan, G. Pereira, U. D. Schwarz, Z. Liu, R. Yamada, W. Dmowski, M. D. Shattuck, C. S. O'Hern, T. Egami, E. Bouchbinder, and J. Schroers, Mechanical glass transition revealed by the fracture toughness of metallic glasses, Nat. Commun. **9**, 3271 (2018).

[11] H. Li, Q. X. Pei, Z. D. Sha, and P. S. Branicio, Intrinsic and extrinsic effects on the fracture toughness of ductile metallic glasses, Mech. Mater. **162**, 104066 (2021).

[12] G. N. Greaves, A. L. Greer, S R. Lakes and T. Rouxel, Poisson's ratio and modern materials, Nat. Mater. **10**, 823 (2011).

[13] J. J. Lewandowski, W. H. Wang, and A. L. Greer, Intrinsic plasticity or brittleness of metallic glasses, Philos. Mag. Lett. **85**, 77 (2005).
[14] B. Deng and Y. Shi, On measuring the fracture energy of model metallic glasses, J. Appl. Phys. **124**, 035101 (2018).
[15] G. Kumar, S. Prades-Rodel, A. Blatter, and J. Schroers, Unusual brittle behavior of Pd-based bulk metallic glass, Scr. Mater. **65**, 585 (2011).
[16] S. V. Madge, D. V. Louzguine-Luzgin, J. J. Lewandowski, and A. L. Greer, Toughness, extrinsic effects and Poisson's ratio of bulk metallic glasses, Acta Mater. **60**, 4800 (2012).
[17] L. Shao, J. Ketkaew, P. Gong, S. Zhao, S. Sohn, P. Bordeenithikasem, A. Datye, R. M. O. Mota, N. Liu, S. A. Kube, Y. Liu, W. Chen, K. Yao, S. Wu, and J. Schroers, Effect of chemical composition on the fracture toughness of bulk metallic glasses, Materialia **12**, 100828 (2020).
[18] S. Plimpton, Fast parallel algorithms for short-range molecular dynamics, J. Comput. Phys. **117**, 1 (1995).
[19] A. P. Thompson, H. M. Aktulga, R. Berger, D. S. Bolintineanu, W. M. Brown, P. S. Crozier, P. J. in 't Veld, A. Kohlmeyer, S. G. Moore, T. D. Nguyen, R. Shan, M. J. Stevens, J. Tranchida, C. Trott, and S. J. Plimpton, LAMMPS - a flexible simulation tool for particle-based materials modeling at the atomic, meso, and continuum scales, Comput. Phys. Commun. **271**, 108171 (2022).
[20] M. Parrinello and A. Rahman, Polymorphic transitions in single crystals: A new molecular dynamics method, J. Appl. Phys. **52**, 7182 (1981).
[21] S. Nosé, A unified formulation of the constant temperature molecular dynamics methods, J. Chem. Phys. **81**, 511 (1984).
[22] Y. Q. Cheng, A. J. Cao, H. W. Sheng, and E. Ma, Local order influences initiation of plastic flow in metallic glass: Effects of alloy composition and sample cooling history, Acta Mater. **56**, 5263 (2008).
[23] W. H. Lin, Y. Teng, Z. D. Sha, S. Y. Yuan, and P. S. Branicio, Mechanical properties of nanoporous metallic glasses: Insights from large-scale atomic simulations, Int. J. Plast. **127**, 102657 (2020).
[24] H. Li, C. G. Jin, and Z. D. Sha, The effect of pressure-promoted thermal rejuvenation on the fracture energy of metallic glasses, J. Non-Cryst. Solids **590**, 121674 (2022).
[25] K. Georgarakis, L. Hennet, G. A. Evangelakis, J. Antonowicz, G. B. Bokas, V. Honkimaki, A. Bytchkov, M. W. Chen, and A. R. Yavari, Probing the structure of a liquid metal during vitrification, Acta Mater. **87**, 174 (2015).
[26] T. Bryk, N. Jakse, G. Ruocco, and J.-F. Wax, Nonacoustic high-frequency collective excitations in a ZrCuAl metallic glass, Phys. Rev. B **106**, 174203 (2022).
[27] D. Ma, A. D. Stoica, X. L. Wang, Z. P. Lu, M. Xu, and M. Kramer, Efficient local atomic packing in metallic glasses and its correlation with glass-forming ability, Phys. Rev. B **80**, 014202 (2009).
[28] N. Mattern, P. Jóvári, I. Kaban, S. Gruner, A. Elsner, V. Kokotin, H. Franz, B. Beuneu, and J. Eckert, Short-range order of Cu–Zr metallic glasses, J. Alloys Compd. **485**, 163 (2009).
[29] N. Mattern, A. Schöps, U. Kühn, J. Acker, O. Khvostikova, and J. Eckert, Structural behavior of Cu_xZr_{100-x} metallic glass ($x = 35-70$), J. Non-Cryst. Solids **354**, 1054 (2008).
[30] L. Li, L. Wang, R. Li, H. Zhao, D. Qu, K. W. Chapman, P. J. Chupas, and H. Liu, Constant real-space fractal dimensionality and structure evolution in $Ti_{62}Cu_{38}$ metallic glass under high pressure, Phys. Rev. B **94**, 184201 (2016).
[31] M. Celtek, Atomic structure of $Cu_{60}Ti_{20}Zr_{20}$ metallic glass under high pressures, Intermetallics **143**, 107493 (2022).
[32] H. L. Peng, M. Z. Li, W. H. Wang, C. Z. Wang, and K. M. Ho, Effect of local structures and atomic packing on glass forming ability in Cu_xZr_{100-x} metallic glasses, Appl. Phys. Lett. **96**, 021901 (2010).
[33] W. Chen, H. F. Zhou, Z. Liu, J. Ketkaew, L. Shao, N. Li, P. Gong, W. Samela, H. J. Gao, and J. Schroers, Test sample geometry for fracture toughness measurements of bulk metallic glasses, Acta Mater. **145**, 477 (2018).
[34] D. Xu, B. Lohwongwatana, G. Duan, W. L. Johnson, and C. Garland, Bulk metallic glass formation in binary Cu-rich alloy series $Cu_{100-x}Zr_x$ ($x = 34$, 36, 38.2, 40 at.%) and mechanical properties of bulk $Cu_{64}Zr_{36}$ glass, Acta Mater. **52**, 2621 (2004).
[35] W. H. Wang, The elastic properties, elastic models and elastic perspectives of metallic glasses, Prog. Mater. Sci. **57**, 487 (2012).
[36] M. I. Mendelev, D. K. Rehbein, R. T. Ott, M. J. Kramer, and D. J. Sordelet, Computer simulation and experimental study of elastic properties of amorphous Cu-Zr alloys, J. Appl. Phys. **102**, 093518 (2007).
[37] J. Schroers and W. L. Johnson, Ductile Bulk Metallic Glass, Phys. Rev. Lett. **93**, 255506 (2004).
[38] F. Shimizu, S. Ogata, and J. Li, Theory of shear banding in metallic glasses and molecular dynamics calculations, Mater. Trans. **48**, 2923 (2007).
[39] Z. P. Lu, H. Tan, Y. Li, and S. C. Ng, The correlation between reduced glass transition temperature and glass forming ability of bulk metallic glasses, Scr. Mater. **42**, 667 (2000).
[40] S. W. Kao, C. C. Hwang, and T. S. Chin, Simulation of reduced glass transition temperature of Cu-Zr alloys by molecular dynamics, J. Appl. Phys. **105**, 064913 (2009).
[41] D. Turnbull and M. H. Cohen, Concerning reconstructive transformation and formation of glass, J. Chem. Phys. **29**, 1049 (1958).
[42] D. D. Wen, P. Peng, Y. Q. Jiang, Z. A. Tian, W. Li, and R. S. Liu, Correlation of the heredity of icosahedral clusters with the glass forming ability of rapidly solidified Cu_xZr_{100-x} alloys, J. Non-Cryst. Solids **427**, 199 (2015).
[43] V. N. Novikov and A. P. Sokolov, Poisson's ratio and the fragility of glass-forming liquids, Nature (London) **431**, 961 (2004).
[44] W. L. Johnson, J. H. Na, and M. D. Demetriou, Quantifying the origin of metallic glass formation, Nat. Commun. **7**, 10313 (2016).
[45] O. N. Senkov, Correlation between fragility and glass-forming ability of metallic alloys, Phys. Rev. B **76**, 104202 (2007).
[46] R. Böhmer, K. L. Ngai, C. A. Angell, and D. J. Plazek, Nonexponential relaxations in strong and fragile glass formers, J. Chem. Phys. **99**, 4201 (1993).
[47] C. Bennemann, J. Baschnagel, and W. Paul, Molecular-dynamics simulation of a glassy polymer melt: Incoherent scattering function, Eur. Phys. J. B **10**, 323 (1999).
[48] W. Kob and H. C. Andersen, Testing mode-coupling theory for a supercooled binary Lennard-Jones mixture. II. Intermediate scattering function and dynamic susceptibility, Phys. Rev. E **52**, 4134 (1995).

[49] Y. Q. Cheng, H. W. Sheng, and E. Ma, Relationship between structure, dynamics, and mechanical properties in metallic glass-forming alloys, Phys. Rev. B **78**, 014207 (2008).

[50] Y. C. Hu, P. F. Guan, Q. Wang, Y. Yang, H. Y. Bai, and W. H. Wang, Pressure effects on structure and dynamics of metallic glass-forming liquid, J. Chem. Phys. **146**, 024507 (2017).

[51] L. Sun, C. Peng, Y. Cheng, K. Song, X. Li, and L. Wang, The structural asymmetry of metallic melts changing with temperature reflects the fragility, J. Non-Cryst. Solids **563**, 120814 (2021).

[52] H. B. Yu, R. Richert, R. Maass, and K. Samwer, Strain induced fragility transition in metallic glass, Nat. Commun. **6**, 7179 (2015).

[53] R. J. Xue, L. Z. Zhao, M. X. Pan, B. Zhang, and W. H. Wang, Correlation between density of metallic glasses and dynamic fragility of metallic glass-forming liquids, J. Non-Cryst. Solids **425**, 153 (2015).

[54] Q. L. Bi and Y. J. LÜ, A kinetic transition from low to high fragility in Cu-Zr liquids, Chin. Phys. Lett. **31**, 106401 (2014).

[55] T. Wang, X. Ma, Y. Chen, J. Qiao, L. Xie, and Q. Li, Structural heterogeneity originated plasticity in Zr-Cu-Al bulk metallic glasses, Intermetallics **121**, 106790 (2020).

[56] Z. D. Zhu, E. Ma, and J. Xu, Elevating the fracture toughness of $Cu_{49}Hf_{42}Al_9$ bulk metallic glass: Effects of cooling rate and frozen-in excess volume, Intermetallics **46**, 164 (2014).

[57] X. K. Xi, D. Q. Zhao, M. X. Pan, W. H. Wang, Y. Wu, and J. J. Lewandowski, Fracture of Brittle Metallic Glasses: Brittleness or Plasticity, Phys. Rev. Lett. **94**, 125510 (2005).

[58] M. B. Tang, D. Q. Zhao, M. X. Pan, and W. H. Wang, Binary Cu-Zr bulk metallic glasses, Chin. Phys. Lett. **21**, 901 (2004).

[59] Q. Zheng, J. Xu, and E. Ma, High glass-forming ability correlated with fragility of Mg-Cu(Ag)-Gd alloys, J. Appl. Phys. **102**, 113519 (2007).

[60] C. Zhang, Q. Chi, J. Zhang, Y. Dong, A. He, X. Zhang, P. Geng, J. Li, H. Xiao, J. Song, and B. Shen, Correlation among the amorphous forming ability, viscosity, free-energy difference and interfacial tension in Fe-Si-B-P soft magnetic alloys, J. Alloys Compd. **831**, 154784 (2020).

[61] M. W. Chen, A brief overview of bulk metallic glasses, NPG Asia Mater. **3**, 82 (2011).

[62] T. Fujita, K. Konno, W. Zhang, V. Kumar, M. Matsuura, A. Inoue, T. Sakurai, and M. W. Chen, Atomic-scale Heterogeneity of a Multicomponent Bulk Metallic Glass with Excellent Glass Forming Ability, Phys. Rev. Lett. **103**, 075502 (2009).

[63] A. J. Cao, Y. Q. Cheng, and E. Ma, Structural processes that initiate shear localization in metallic glass, Acta Mater. **57**, 5146 (2009).

[64] Y. Q. Cheng, A. J. Cao, and E. Ma, Correlation between the elastic modulus and the intrinsic plastic behavior of metallic glasses: The roles of atomic configuration and alloy composition, Acta Mater. **57**, 3253 (2009).